THE JOURNAL OF PHYSICAL CHEMISTRY LETTERS
A JOURNAL OF THE AMERICAN CHEMICAL SOCIETY

pubs.acs.org/JPCL

Letter

Dichroic Photoelasticity in Black Phosphorus Revealed by Ultrafast Coherent Phonon Dynamics

Simin Wu,[⊥] Zixuan Lu,[⊥] Anqi Hu, Xianchong Miao, Fanjie Wang, Zhengzong Sun, Hugen Yan, Hao Zhang,* and Minbiao Ji*

Cite This: *J. Phys. Chem. Lett.* 2021, 12, 5871−5878

Read Online

ACCESS | Metrics & More | Article Recommendations | Supporting Information

ABSTRACT: Coherent longitudinal lattice vibrations of black phosphorus provide unique access to the out-of-plane strain coupled in-plane optical properties. In this work, polarization-resolved femtosecond transient absorption microscopy is applied to study the anisotropic coherent phonon responses. Multiorder phonon harmonics were observed with thickness dependence well explained by the linear chain model, allowing rapid optical mapping of phonon frequency distributions. More interestingly, exotic coherent phonon oscillations occurred with a π-phase jump between the armchair and zigzag polarizations, which reveals opposite signs of photoelasticity under the longitudinal strain. Specifically, compressive strain reduces the imaginary refractive index in the armchair polarization but increases the real refractive index in the zigzag polarization, as confirmed by the ab initio calculations and thin film model. These fundamental properties of black phosphorus hold potential for applications in ultrafast and polarization-sensitive photoacoustic/photoelastic modulators.

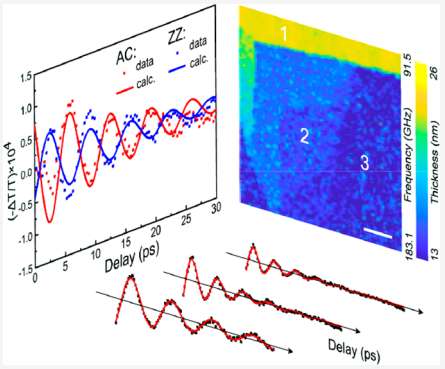

Black phosphorus (BP) has attracted growing interest among the 2D family because of not only its excellent layer-dependent electronic and optical properties[1−6] but also the strong anisotropic behavior due to the puckered honeycomb structure with armchair (AC) and zigzag (ZZ) features, including optical,[7−10] mechanical[11,12] and electric properties.[1,11] Most extensively studied were the static in-plane strain-induced anisotropies.[2,13] On the other hand, out-of-plane strain coupled in-plane anisotropy also results in peculiar properties, such as the negative Poisson ratio of BP, as shown in theoretical calculations.[14] Experimental investigations of the longitudinal strain-induced optical anisotropy in BP are more challenging yet expected to provide a fundamental understanding of the photoelasticity, as well as the modulation of optical dichroism through coherent dynamic strain pulses.

Lattice vibration (phonon) of BP provides a unique means to study its elasto-optical properties,[15,16] because of the strong electron−phonon and interlayer couplings.[17,18] Vibrational properties of 2D materials have usually been studied with conventional Raman spectroscopy, especially for the high-frequency optical phonons as in graphene, molybdenum disulfide (MoS_2), and BP.[19] Low-frequency optical phonons and acoustic phonons are more difficult to measure with conventional Raman scattering[20] and could be alternatively observed by femtosecond pump−probe spectroscopy in the time domain.[21,22] In these experiments, impulsive laser excitation (pump) generates collective motion of lattice vibrations known as coherent phonons (CPs), which modify the local dielectric function that further modulates the probe pulse intensity, via either differential reflection ($\Delta R/R$) or differential transmission ($\Delta T/T$).[21,23,24] Time-resolved CP dynamics reveals the embedded information on phonon frequency, damping time, and oscillation phase. More importantly, coherent longitudinal acoustic phonons (CLAPs) generate dynamic out-of-plane strain waves,[25] providing a unique opportunity to investigate the longitudinal strain-induced in-plane optical properties in BP, especially the polarization sensitivity of the photoelastic responses and its ultrafast dynamical behaviors that may have potential application for high-speed modulators.

In this work, we applied femtosecond transient absorption microscopy to study the thickness- and polarization-dependent coherent phonon dynamics in BP films with thickness ranging from a few layers to 400 nm. A common CLAP mode has dominated the transient optical behavior of BP below 200 nm thickness, agreeing with the strong electron−phonon coupling effects and selection rules for transient optical measurements. Moreover, anisotropic CP oscillations with a π-phase jump between the AC and ZZ directions were observed in BP films with a thickness of around 5−30 nm, indicating opposite signs of longitudinal strain-induced transmission. This revealed

Received: May 6, 2021
Accepted: June 16, 2021
Published: June 18, 2021

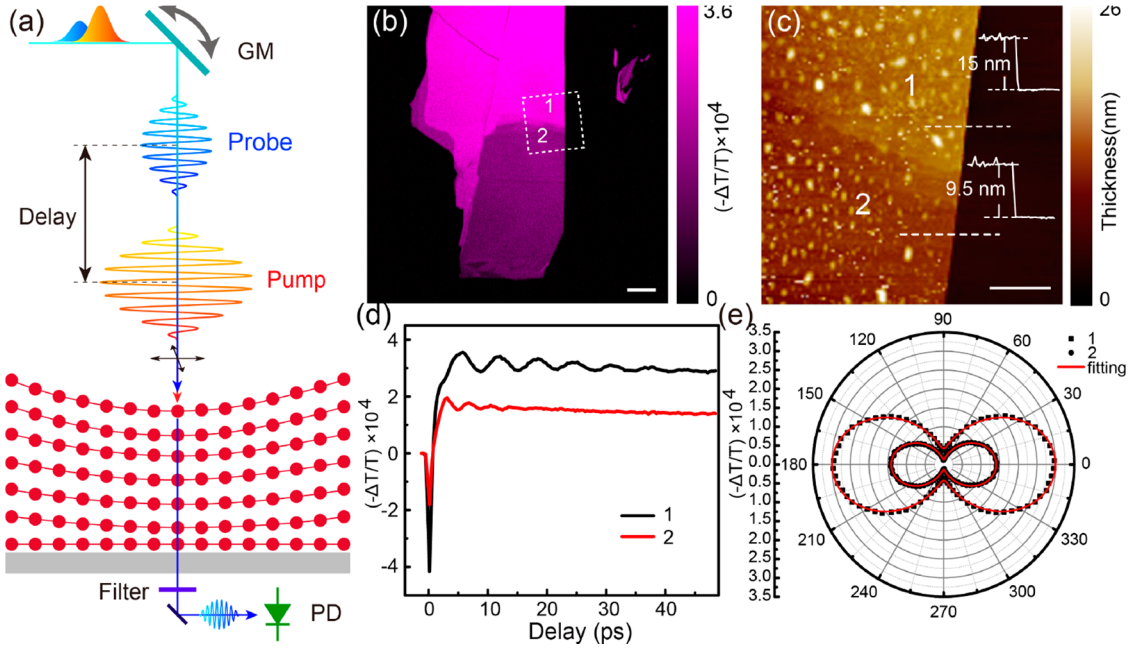

Figure 1. Characterization of black phosphorus flakes with ultrafast pump−probe microscopy. (a) Illustration of the excitation and detection of coherent phonons with pump−probe microscopy. (b) Transient absorption image taken at 5.5 ps time delay. (c) Atomic force microscopy image of the same sample in the dashed square region. (d) Representative transient absorption dynamics in the two thickness regions. (e) Anisotropic TA signal. Scale bar: b, 10 μm; c, 4 μm.

opposite photoelastic properties in the AC and ZZ directions of BP, as confirmed by our calculations and theoretical model.

The home-built laser-scanning femtosecond pump−probe microscope (Supporting Information) was used to detect the transient absorption (TA) signal with spatial resolution of ∼350 nm and temporal resolution of ∼200 fs.[24] The TA signal ($-\Delta T/T$) was collected pixel by pixel as the focused laser spot raster scanned across the sample to generate a stack of images at varying time delay (τ) between pump and probe pulses (Figure 1a and Figure S1). The three-dimensional data (x, y, τ) allows us to extract the transient dynamics of any chosen spatial region in the sample. Compared with traditional TA spectroscopy with fixed laser spots, our rapid and high-throughput method is advantageous in avoiding photodamage for BP samples. Unless specifically stated, both beams were polarized in parallel, and their polarizations could be rotated by a half-wave plate mounted in a motorized rotational stage (K10CR1, Thorlabs). BP flake samples were prepared by mechanical exfoliation onto a transparent polydimethylsiloxane (PDMS, Gel-Pak) substrate for direct TA measurements or further transferred onto fused silica substrates (roughness <1 nm) for atomic force microscopy (AFM) measurements for thickness characterizations. IR absorption measurements were conducted to determine the crystal orientation, which were found to be consistent with our polarization-dependent TA results. Throughout the work, we assigned AC and ZZ crystal orientations to 0 and 90°, respectively.

Parts b and c of Figure 1 show the TA and AFM images of a typical BP flake, all of which demonstrate roughly two regions of thicknesses. The AFM image of the dashed square area reveals these regions with thicknesses of 15 and 9.5 nm (Figure 1c), which demonstrate different transient behaviors, as shown in Figure 1d and Supporting Movie S1. Akin to the results of few-layer BP, each TA curve is composed of the carrier dynamics with fast (∼1.2 ps) and slow relaxations (∼230 ps)[21,24] and clear CP oscillations with large amplitude (>10% of total TA signal), indicating strong electron−phonon coupling. In contrast to few-layer BP, these thin films do not exhibit excitonic resonances and hence we would rather focus on the coherent phonons than the carrier dynamics in this study. Figure 1e shows the polarization-dependent TA signal which exhibits typical anisotropic distributions and could be used to determine the lattice orientations of BP samples. Pump laser power dependence shows a linear relationship with CP amplitude at low excitation power (Figure S2), which agrees with the mechanism of CP generation by the deformation potential effect (DPE).[26,27] Note that the CP amplitude in the AC direction is more prone to saturate with increasing pump power than in the ZZ direction, because of the strong anisotropic optical absorption of BP films.

We first investigated the oscillation frequency of BP samples with thickness ranging from 7 to 400 nm. Notice that CP frequency is independent of laser polarization, and to extract the oscillation frequency from the TA curves, we fitted the data with an empirical function containing both the carrier and CP dynamics (Supporting Information). Representative data and fitting results of the extracted CP components with different thicknesses are shown in Figure 2a. We plotted CP period T of all the measured samples with thickness (d) ranging from 7 to 150 nm, which exhibits a linear relation that could be well fitted by $T = 2d/\nu$, as described in the one-dimensional (1D) standing wave model with boundary condition of zero strains at both ends.[28,29] Here ν is the acoustic velocity in BP, which is estimated to be ∼4.87 ± 0.05 km/s according to the fitting result, agreeing well with the time domain thermos-reflectance (TDTR) measurement[30] and our calculation result (Supporting Information).

To include the results of few-layer BP,[24] the layer dependence of CP frequency is better described by the 1D chain model of the layer breathing mode (LBM),[17,20,31]

https://doi.org/10.1021/acs.jpclett.1c01463
J. Phys. Chem. Lett. 2021, 12, 5871−5878

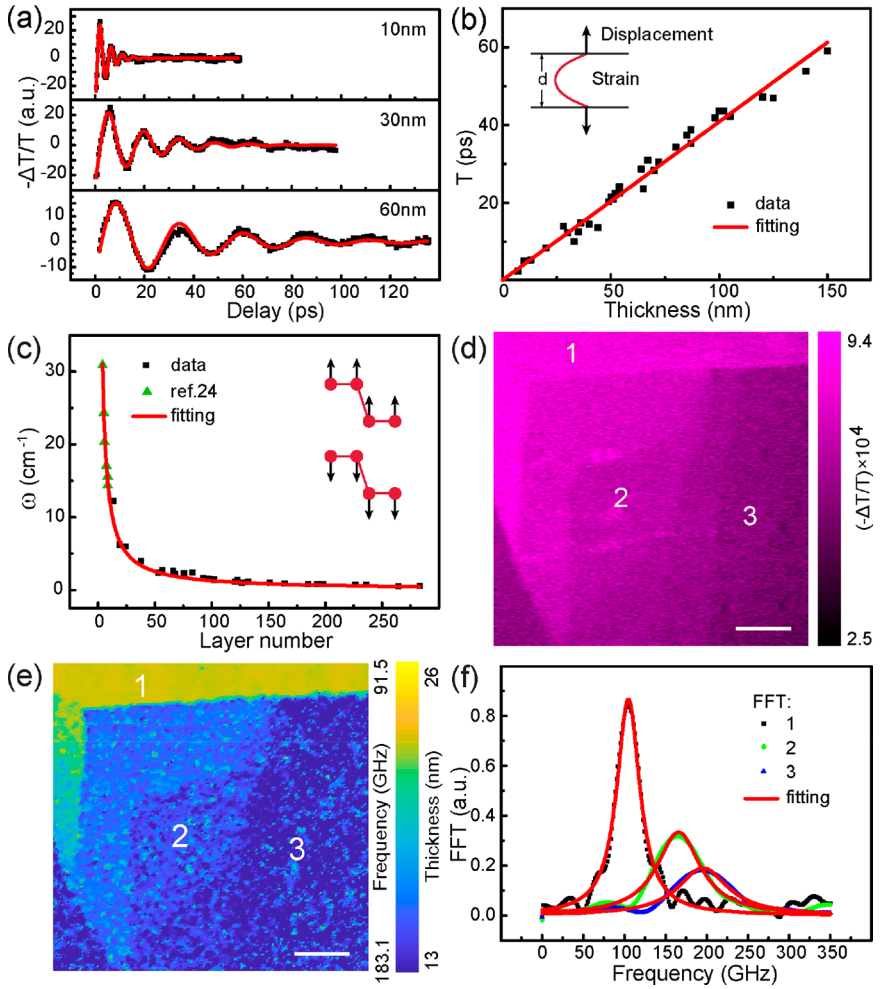

Figure 2. Thickness-dependent coherent phonon oscillations and imaging phonon frequency distributions. (a) Extracted coherent phonon dynamics in 10, 30, and 60 nm thick BP flakes. (b) Thickness-dependent oscillation periods fitted with the 1D standing wave model. (Reproduced with permission.[24] Copyright 2018 American Chemical Society.) (c) Layer-dependent oscillation frequency fitted with the 1D chain model. (d) TA intensity map of a BP flake and (e) the corresponding phonon frequency (thickness) distributions. (f) FFT results of the three thickness regions. Scale bar: 5 μm.

expressed as $\omega_N = \omega_0\sqrt{1 - \cos\frac{n\pi}{N}}$. Here, N refers to the layer number, n is the order of the vibrational harmonics (n = 1 applies to the fundamental mode). The 1D chain model successfully fit all of the CP frequencies from four layers to 150 nm (Figure 2c) with ω_0 = 57 cm^{-1}, agreeing with the previous result.[24] It thus implies that the CP mode for all of the BP samples within the thickness range is essentially the same LBM. The 1D chain model converges to the common 1D standing wave model when N gets larger as in thicker samples, and the corresponding oscillation period becomes $T \cong \frac{\sqrt{2}d}{\pi c\omega_0 a_0} = \frac{2d}{\nu}$ ($N \gg 1$). The acoustic velocity could thus be written as $\nu = \sqrt{2}\pi c\omega_0 a_0$, where a_0 is the thickness of single-layer BP (lattice constant) and the phonon frequency has been converted into wavenumber (cm^{-1}). Using a_0 = 0.53 nm from the literature,[32] the 1D chain model gives an acoustic velocity of ν = 4.03 km/s, agreeing well with our calculation result (Supporting Information). In fact, the classic monatomic linear chain model infers a linear phonon dispersion under long wave approximation ($\lambda \gg a_0$),[33] resulting in standing waves with open boundary conditions. However, in the short wave limit ($\lambda \sim a_0$), the dispersion linearity breaks as it approaches the boundaries of the Brillouin zone, which is the case in few-layer samples.

The T−d relationship allows us to image the sample thickness with TA microscopy, especially for BP flakes on soft substrates such as PDMS, which is difficult to measure accurately with AFM. In addition to the intensity map of BP flakes (Figure 2d), the thickness distribution (Figure 2e) could be extracted by analyzing the oscillation frequency ω_N using fast Fourier transformation (FFT) pixel-by-pixel and converting ω_N to thickness d. Representative FFT results of three thickness regions are plotted in Figure 2f with Lorentzian line shape fitting. This has potential application in rapid and high-throughput characterization of sample thickness within the 10−200 nm range, where IR spectra start to lose excitonic features for thickness characterization and AFM measurements become limited by the slow speed and small scan area. In our setup, a 200 × 200 μm^2 sized BP flake usually costs about 3 min to image with TA microscopy (512 × 512 pixels) to capture the CP oscillations.

In BP films much thicker than the estimated penetration depth of ∼250 nm,[32] heat stress and coherent phonons are generated near the front surface and propagate through the sample, forming Brillouin oscillations with thickness-independ-

https://doi.org/10.1021/acs.jpclett.1c01463
J. Phys. Chem. Lett. 2021, 12, 5871−5878

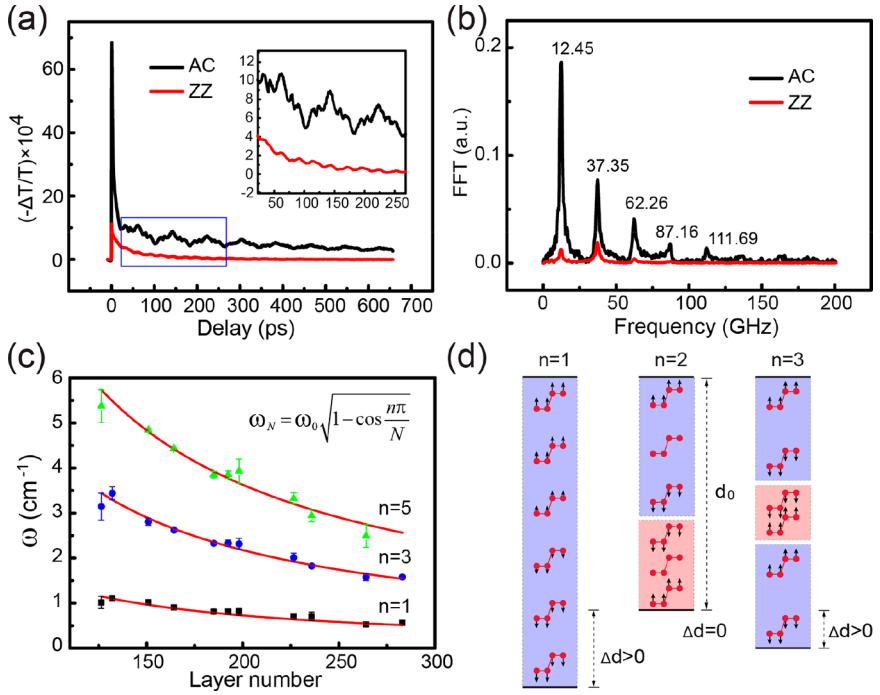

Figure 3. Multiorder phonon harmonics in thick BP. (a) Higher-order phonon harmonics and dynamics in AC and ZZ directions with an enlarged view shown in the inset. (b) Corresponding FFT results of harmonic frequencies. (c) Layer-dependent harmonic frequencies (n = 1, 3, 5) fitted with the 1D chain model. (d) Illustration of atomic displacements in six-layer BP for the layer breathing mode with harmonics of 1−3.

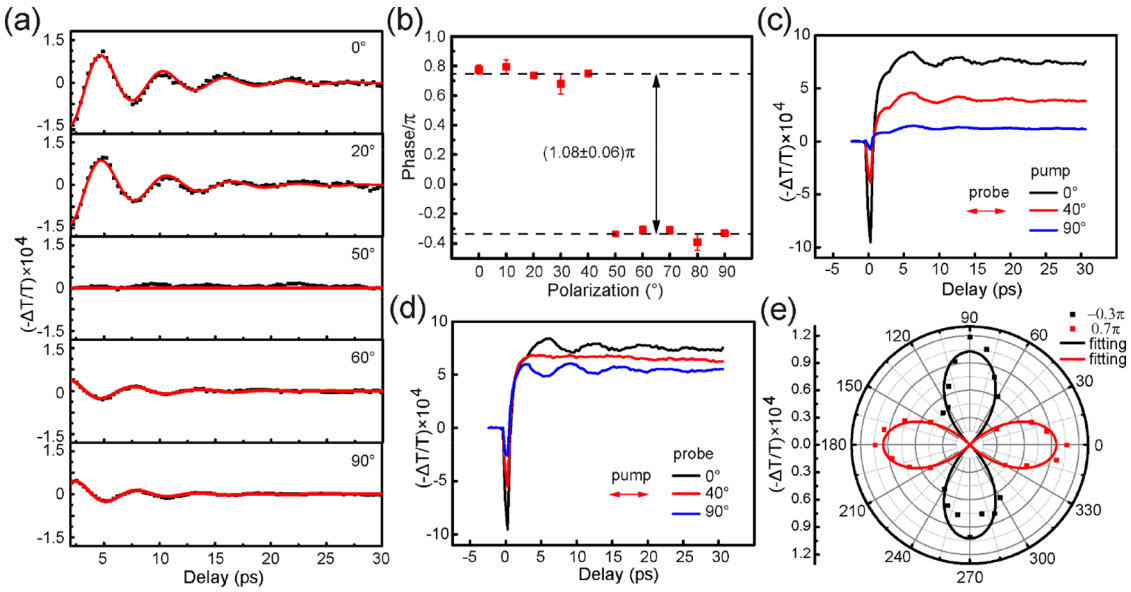

Figure 4. Polarization dependence of phonon oscillation phases. (a) Coherent phonon dynamics with pump and probe polarizations simultaneously varied from AC (0°) to ZZ (90°). (b) The extracted oscillation phases at different polarization angles. (c) TA dynamics with varying pump polarization while the probe beam was fixed along AC polarization. (d) TA dynamics with varying probe polarization while the pump beam was fixed along AC polarization. (e) Probe-polarization-dependent CP amplitude, with opposite signs color-coded.

ent frequency (~42 GHz).[21,34] In this case, the oscillation period could be written as $T = \lambda/2n\nu$, where λ is the probe wavelength, ν is the acoustic velocity, and n is the refraction index. Typical results of Brillouin oscillation could be found in Figure S3, which agrees with the work of Meng et al.[35]

As predicted in the 1D chain model, higher-order harmonic modes (n > 1) should also exist in the generation process of coherent phonons, yet they require specific selection rules and sufficient electron−phonon couplings to be detected optically. We observed multiorder harmonics mostly in BP samples thicker than 60 nm, with a typical result shown in Figure 3a (~190 nm thick). In both the AC and ZZ directions, the TA dynamics show not only the fundamental oscillations of the ~80 ps period but also higher frequency components that add up together to synthesize the overall TA behavior to appear "triangular wave"-like (Figure 3a), "square wave"-like, and like other waveforms (Figure S4). FFT analysis revealed that only odd-order harmonics could be detected with TA measure-

https://doi.org/10.1021/acs.jpclett.1c01463
J. Phys. Chem. Lett. 2021, 12, 5871−5878

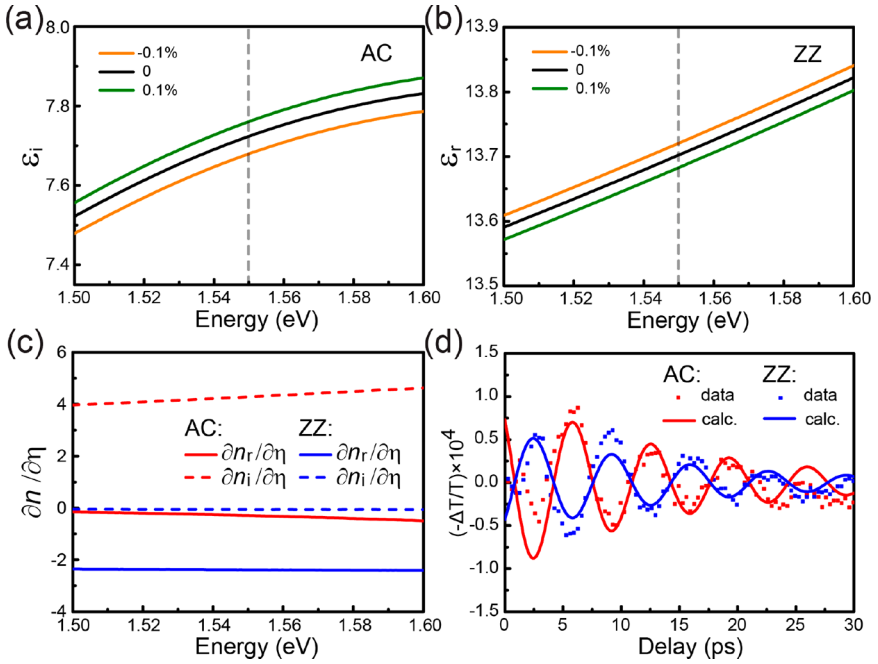

Figure 5. Photoelasticity of BP and its relation with phonon oscillation phases. (a, b) Calculated imaginary part of the dielectric function in AC and the real part in the ZZ direction under longitudinal strains of 0, ±0.1%. (c) Calculated photoelastic coefficients in both directions. (d) Simulated transient coherent phonon responses in AC and ZZ.

ments (Figure 3b), and up to ninth order harmonics could be seen in the spectra, with perfect linearity between frequency and order number (Figure S5). Although anisotropic CP features exist in the FFT spectra between AC and ZZ, they share the same frequencies except that ZZ tends to cut off at relatively lower orders. Moreover, all thickness-dependent CP frequencies for n = 1, 3, and 5 could be globally fitted by the 1D chain model (Figure 3c), with the fitting result of ω_0 = 65.4 ± 0.3 cm^{-1} (corresponds to v = 4.62 km/s).

The selection rule that only odd orders of phonon harmonics could be detected with TA can be explained by the resonant acoustic cavity effect for discrete acoustic phonon modes.[22,36] As illustrated in Figure 3d, the acoustic cavity essentially results in standing waves along the z direction with zero strains at both surfaces. Therefore, in the fundamental mode (n = 1), the total volume (thickness) undergoes periodic expansion and contraction that modulates the transmission intensity of the probe beam through the photoelastic effect, which is also true for other odd orders (such as n = 3) with nonzero changes of the total volume. However, in even orders (such as n = 2), no net change of volume occurs because of the cancellation between the equal number of subsets with opposite displacements, and this thus contributes little to the TA signal. In addition to the above detection selection rule, the excitation process may also favor the symmetric odd modes other than the antisymmetric even ones, because of the homogeneous heat stress in thin films that generates predominantly symmetric lattice strain field.[22,37]

Optical anisotropy of black phosphorus is commonly seen in both linear and nonlinear optics,[9] mainly attributed to anisotropic lattice structures that lead to polarization-dependent optical responses coupled with electronic transitions. Vibrational transitions also demonstrated strong anisotropy through electron−phonon couplings, as shown in Raman and CP studies of few-layer BP.[19,24,38] In contrast to the phenomena observed in few-layer BP where the amplitude of CP shows resonance enhancement in the AC direction and vanishes in ZZ, thicker BP films with thickness ranging from 5 to 30 nm exhibit more exotic coherent phonon behaviors, especially the out-of-phase oscillation of CP dynamics along the two orthogonal directions, from which we could extract the anisotropic photoelasticity of acoustic−optical coupling.

As shown in a typical BP flake of ∼16 nm thickness, the time-domain CP oscillation undergoes a π-phase jump when the beam polarizations collinearly changed from the AC (0°) to ZZ (90°) direction (Figure 4a and b). In order to understand the mechanism, we performed separate polarization-dependent measurements. With fixed probe polarization (in AC), only the amplitudes of CP and photocarrier responses changed proportionally with varying pump polarization, yet no variation of the phonon oscillation phase was seen (Figure 4c). In contrast, when the pump polarization was maintained (in AC), CP oscillations demonstrated a clear out-of-phase transition between the two perpendicular probe polarizations (Figure 4d). More detailed pump- and probe-polarization-dependent TA data could be found in Figure S6. Probe-polarization-resolved CP amplitude is shown in the polar chart (Figure 4e), with different colors representing opposite signs of oscillation amplitudes (π-phase shift). Considering CLAP generates strains in the z direction, we hypothesized that the breathing of the sample thickness may induce opposite changes of probe absorbance in AC and ZZ polarizations, resulting in the out-of-phase oscillations of the differential transmission signal of the probe beam. However, the pump beam mainly contributes to the density of excited coherent phonons and photocarriers.

We then quantitatively evaluated the coherent acoustic phonon-induced TA signal of BP thin film on PDMS substrate. In the conventional Brillouin scattering process with photon energy below the bandgap, only the real part of the refractive index accounts for the CP signal in transient reflectivity.[39] However, in our case, the probe photon energy is above the BP

https://doi.org/10.1021/acs.jpclett.1c01463
J. Phys. Chem. Lett. 2021, 12, 5871−5878

bandgap and electronic transitions from valence bands to conduction bands contribute largely to the TA signal; hence, both the real and imaginary parts of the complex refractive index and photoelastic coefficient need to be included. Combining the general perturbative approach in bulk material developed by Thomsen[34] and multireflection/interference effects in thin film, the strain-induced transient absorbance could be approximated as

$$-\frac{\Delta T}{T} \cong 2\mathrm{Im}\left[\left(t_1 - \frac{2r_0 r_1 e^{2i\delta_0}}{1 + r_0 r_1 e^{2i\delta_0}}\right) k_0 \frac{\partial \tilde{n}}{\partial \eta_{33}} \int_0^d \eta_{33}(z, t)\, dz\right] \quad (1)$$

where k_0 denotes the probe wave vector in a vacuum, $\tilde{n} = n_r + in_i$ is the complex refractive index of BP, r_0 represents the amplitude reflection coefficient at the air/BP interface, r_1 and t_1 represent the amplitude reflection and transmission coefficient at the BP/PDMS interface, and $\delta_0 = k_0 \tilde{n} d$ is the complex phase of probe light traveling through BP film of thickness d. Thin film approximation has been made to simplify the equation ($d \ll \lambda$), and detailed formula deductions could be found in the Supporting Information.

The expression of eq 1 has considered contributions of multiple reflection, transmission, absorption, and backscattering from inhomogeneous distribution of refractive index induced by the time-dependent longitudinal coherent strain field $\eta_{33}(z, t)$. The electron−phonon coupling strength that determines the CP amplitude is hidden in the complex photoelastic coefficient $P_{i3} = \partial \tilde{n}/\partial \eta_{33}$ (i = 1,2), which is independent of strain in the linear regime (small strain on the order of $\eta_{33} \sim 10^{-4}$), and the anisotropic behavior of CP oscillation is linked to the anisotropy of the photoelasticity. Although we focus on the fundamental phonon mode, it can be immediately seen from eq 1 that even-order phonon harmonics do not contribute to the transient signal because the spatial integral of the antisymmetric strain field $\eta_{33}(z, t)$ vanishes. Since the photoelastic coefficients of BP film in the near-infrared probe wavelength range are unknown, we rely on the *ab initio* calculation results based on the density functional theory (DFT) method. The computational details related to the DFT calculations are shown in the Supporting Information.

We computed the strain-induced changes of the complex dielectric function ($\varepsilon = \varepsilon_r + i\varepsilon_i$) of 16 nm thick BP film in both AC and ZZ polarizations under longitudinal strains η_{33} of 0, ±0.1% (Figure 5a,b and Figure S7) as well as the photoelastic coefficients $\partial \tilde{n}/\partial \eta_{33}$ (Figure 5c). Our results show that, at 800 nm (1.55 eV), only the imaginary photoelastic coefficient $\partial n_i/\partial \eta_{33}$ in the AC direction has a positive sign, opposite to all of the other three coefficients (Figure 5c). It is also shown that the photoelasticity in the AC direction is dominated by the imaginary part, while the ZZ direction is dominated by the real part. The opposite signs indicate that compressive/tensile strain leads to decreased/increased imaginary refractive index in AC and increased/decreased real refractive index in the ZZ direction. For ∼16 nm BP film generating transient signal $-\Delta T/T \sim 10^{-4}$, a longitudinal standing wave with strain amplitude $\eta_{33} \sim -10^{-4}$ is estimated that could well reproduce the experimental data by our model in eq 1, including both the amplitude and phase relationships of the damped CP oscillations (∼15 ps damping time) between AC and ZZ directions (Figure 5d). The negative sign of η_{33} suggests compressive stress induced by photoexcitation. On the basis of bulk deformation potentials and elastic properties of BP, we can also calculate the photoinduced longitudinal strain $\eta_{33} = (d_e + d_h)N_c/\rho_0 v^2 \sim -10^{-4}$, in agreement with our model. Here d_e and d_h are the deformation potentials ($d_e + d_h = B\partial E_g/\partial P$ = −6.44 eV),[40] B = 36 GPa is the bulk modulus, N_c is the photoexcited carrier density, ρ_0 is the mass density, and v is the acoustic velocity. Although the simple model offers a thickness-dependent description, the CP phase information becomes more complex in thicker films due to the interference of higher-order phonon harmonics and the deviation from thin-film approximation, whereas the excitonic resonance effect becomes dominant in few-layer BP. Hence, the anisotropic out-of-phase oscillation phenomenon is most reliably shown in samples within the thickness range of 5−30 nm.

The π-phase shift of coherent phonons has been observed in other semiconductors and superlattices[26,41,42] but with different phenomena and underlying physical mechanisms. These include the pump-power-induced changes of built-in electric field;[41] the competition between the deformation potential effect and the inverse piezoelectric effect that generated opposite signs of transient signals with different pump power;[43] and the strain-induced shift of bandgap that yields opposite signs of differential signal when the probe photon energy varied across the bandedge.[26] In contrast, the π-phase shift in thin BP film is caused by the opposite photoelasticity along the two orthogonal lattice orientations, which is seldom seen in other materials.

Static strain-induced changes of BP optical properties have been investigated mostly with in-plane methods produced by stretching/bending of substrates.[13] Complimentarily, coherent longitudinal acoustic phonons allow us to investigate the out-of-plane strain coupled in-plane optical properties. Our finding that the out-of-plane strain induces opposite changes of refractive index may be related to the negative Poisson ratio of each BP layer; i.e., compressive longitudinal strain induces tension along the AC direction but compression along the ZZ direction,[14] resulting in opposite changes of dielectric responses in the two polarizations. Given the ultrafast time scale of the coherent phonons (∼200 GHz), the dichroic photoelasticity of BP may have promising device applications for ultra-high-speed and polarization-selective photoelastic or photoacoustic modulators, that allow the tuning of modulation phase/amplitude by rotating the light polarization or device orientation. Besides, we noticed that the photoelastic anisotropy of BP has little dependence on the probe wavelength within our tuning range (Figure S8).

It is worth discussing the boundary conditions of lattice motions in BP films. The open boundary condition (stress-free at both surfaces) is clearly satisfied in free-standing films,[22] which leads to standing wave with phonon period expressed in $T = 2d/v$. However, for thin films on substrates, different boundary conditions may be required. For instance, in MoS_2/Si and As_2Te_3/SiO_2, zero-displacement boundary condition is satisfied at the material/substrate interface (the other surface remains free), resulting in $T = 4d/v$.[21,28] However, in Au/BK7 glass and BP/SiO_2, the results are the same as in free-standing films.[44] The difference is originated from the acoustic mismatch between material and substrate.[37] In our BP case, SiO_2 and PDMS substrates correspond to "soft substrate"; hence, the coherent phonons share similar frequencies as in suspended films, as shown in our experimental results (Figure S9).

In summary, we have systematically studied the coherent phonon behaviors of BP films in a wide thickness range using

https://doi.org/10.1021/acs.jpclett.1c01463
J. Phys. Chem. Lett. 2021, 12, 5871−5878

ultrafast pump−probe microscopy. The strong electron−phonon coupling has enabled observation of multiharmonics of phonon modes. We found the thickness dependence of these harmonic frequencies could be thoroughly described by the standard 1D chain model, confirming that the layer breathing mode is commonly shared in the coherent phonons from few-layer to ∼200 nm thick samples. Furthermore, we demonstrated anisotropic coherent oscillations with a π-phase difference between the AC and ZZ polarizations and revealed peculiar photoelasticity, as verified with numerical calculations. These results have potential applications in rapid characterization of BP thin films as well as in nanomechanic, photoelastic, and piezochromic devices.

■ ASSOCIATED CONTENT

Supporting Information

The Supporting Information is available free of charge at https://pubs.acs.org/doi/10.1021/acs.jpclett.1c01463.

Experimental setup and methods; power and polarization dependence; Brillouin oscillations; linear fitting between frequency and order number; wavelength dependence; calculated dielectric function; computational details; formula deduction of the thin film model (PDF)

Transient coherent phonon dynamics (AVI)

■ AUTHOR INFORMATION

Corresponding Authors

Hao Zhang − *School of Information Science and Technology, Fudan University, Shanghai 200433, China;* orcid.org/0000-0002-8201-3272; Email: zhangh@fudan.edu.cn

Minbiao Ji − *State Key Laboratory of Surface Physics and Department of Physics, Key Laboratory of Micro and Nano Photonic Structures (Ministry of Education), Fudan University, Shanghai 200433, China; Academy for Engineering and Technology, Human Phenome Institute, Multiscale Research Institute of Complex Systems, Fudan University, Shanghai 200433, China;* orcid.org/0000-0002-9066-4008; Email: minbiaoj@fudan.edu.cn

Authors

Simin Wu − *State Key Laboratory of Surface Physics and Department of Physics, Key Laboratory of Micro and Nano Photonic Structures (Ministry of Education), Fudan University, Shanghai 200433, China*

Zixuan Lu − *School of Information Science and Technology, Fudan University, Shanghai 200433, China*

Anqi Hu − *Department of Chemistry, Fudan University, Shanghai 200433, China*

Xianchong Miao − *State Key Laboratory of Surface Physics and Department of Physics, Key Laboratory of Micro and Nano Photonic Structures (Ministry of Education), Fudan University, Shanghai 200433, China;* orcid.org/0000-0001-5045-3698

Fanjie Wang − *State Key Laboratory of Surface Physics and Department of Physics, Key Laboratory of Micro and Nano Photonic Structures (Ministry of Education), Fudan University, Shanghai 200433, China*

Zhengzong Sun − *Department of Chemistry, Fudan University, Shanghai 200433, China;* orcid.org/0000-0002-3710-4001

Hugen Yan − *State Key Laboratory of Surface Physics and Department of Physics, Key Laboratory of Micro and Nano Photonic Structures (Ministry of Education), Fudan University, Shanghai 200433, China;* orcid.org/0000-0001-8423-6069

Complete contact information is available at: https://pubs.acs.org/10.1021/acs.jpclett.1c01463

Author Contributions

$^{\perp}$S.W., Z.L.: These authors contributed equally.

Author Contributions

M.J. conceived the experiment, Z.L. and H.Z. conducted the numerical calculations, S.W. and X.M. prepared the samples and performed the microscopy measurements, A.H. and Z.S. provided help in the AFM measurements, and F.W. and H.Y. helped with the sample characterization. The manuscript was written by S.W. and M.J. and revised by all authors. All authors have given approval to the final version of the manuscript.

Notes

The authors declare no competing financial interest.

■ ACKNOWLEDGMENTS

We acknowledge the financial support from National Key R&D Program of China (2016YFA0203900); National Natural Science Foundation of China (81671725, 61975033); Shanghai Municipal Science and Technology Major Project (2017SHZDZX01 and 2018SHZDZX01) and ZJLab; and Specialized Research Project of the Shanghai Health and Family Planning Commission on Smart Medicine (2018ZHYL0204). Part of the experiment including the substrate and sample preparation was done in Fudan Nanofabrication Laboratory.

■ REFERENCES

(1) Li, L.; Kim, J.; Jin, C.; Ye, G. J.; Qiu, D. Y.; da Jornada, F. H.; Shi, Z.; Chen, L.; Zhang, Z.; Yang, F.; et al. Direct Observation of the Layer-dependent Electronic Structure in Phosphorene. *Nat. Nanotechnol.* **2017**, *12* (1), 21−25.

(2) Zhang, G. W.; Huang, S. Y.; Chaves, A.; Song, C. Y.; Ozcelik, V. O.; Low, T.; Yan, H. G. Infrared Fingerprints of Few-layer Black Phosphorus. *Nat. Commun.* **2017**, *8*, 14071.

(3) Tran, V.; Soklaski, R.; Liang, Y. F.; Yang, L. Layer-controlled Band Gap and Anisotropic Excitons in Few-layer Black Phosphorus. *Phys. Rev. B* **2014**, *89* (23), 235319.

(4) Zhang, G. W.; Chaves, A.; Huang, S. Y.; Wang, F. J.; Xing, Q. X.; Low, T.; Yan, H. G. Determination of Layer-dependent Exciton Binding Energies in Few-layer Black Phosphorus. *Sci. Adv.* **2018**, *4* (3), eaap9977.

(5) Wang, X. M.; Jones, A. M.; Seyler, K. L.; Tran, V.; Jia, Y. C.; Zhao, H.; Wang, H.; Yang, L.; Xu, X. D.; Xia, F. N. Highly Anisotropic and Robust Excitons in Monolayer Black Phosphorus. *Nat. Nanotechnol.* **2015**, *10* (6), 517−521.

(6) Liu, H.; Neal, A. T.; Zhu, Z.; Luo, Z.; Xu, X. F.; Tomanek, D.; Ye, P. D. Phosphorene: An Unexplored 2D Semiconductor with a High Hole Mobility. *ACS Nano* **2014**, *8* (4), 4033−4041.

(7) Mao, N. N.; Tang, J. Y.; Xie, L. M.; Wu, J. X.; Han, B. W.; Lin, J. J.; Deng, S. B.; Ji, W.; Xu, H.; Liu, K. H.; et al. Optical Anisotropy of Black Phosphorus in the Visible Regime. *J. Am. Chem. Soc.* **2016**, *138* (1), 300−305.

(8) Schuster, R.; Trinckauf, J.; Habenicht, C.; Knupfer, M.; Buchner, B. Anisotropic Particle-hole Excitations in Black Phosphorus. *Phys. Rev. Lett.* **2015**, *115* (2), 026404.

(9) Wang, X.; Lan, S. Optical Properties of Black Phosphorus. *Adv. Opt. Photonics* **2016**, *8* (4), 618−655.

(10) Li, D. A.; Jussila, H.; Karvonen, L.; Ye, G. J.; Lipsanen, H.; Chen, X. H.; Sun, Z. P. Polarization and Thickness Dependent Absorption Properties of Black Phosphorus: New Saturable Absorber for Ultrafast Pulse Generation. *Sci. Rep* **2015**, *5*, 15899.
(11) Tao, J.; Shen, W. F.; Wu, S.; Liu, L.; Feng, Z. H.; Wang, C.; Hu, C. G.; Yao, P.; Zhang, H.; Pang, W.; et al. Mechanical and Electrical Anisotropy of Few-layer Black Phosphorus. *ACS Nano* **2015**, *9* (11), 11362−11370.
(12) Jiang, J.-W.; Park, H. S. Mechanical Properties of Single-layer Black Phosphorus. *J. Phys. D: Appl. Phys.* **2014**, *47* (38), 385304.
(13) Huang, S. Y.; Zhang, G. W.; Fan, F. R.; Song, C. Y.; Wang, F. J.; Xing, Q. X.; Wang, C.; Wu, H.; Yan, H. G. Strain-tunable van Der Waals Interactions in Few-layer Black Phosphorus. *Nat. Commun.* **2019**, *10*, 2447.
(14) Jiang, J. W.; Park, H. S. Negative Poisson's Ratio in Single-layer Black Phosphorus. *Nat. Commun.* **2014**, *5*, 4727.
(15) Luer, L.; Gadermaier, C.; Crochet, J.; Hertel, T.; Brida, D.; Lanzani, G. Coherent Phonon Dynamics in Semiconducting Carbon Nanotubes: A Quantitative Study of Electron-phonon Coupling. *Phys. Rev. Lett.* **2009**, *102* (12), 127401.
(16) Luckyanova, M. N.; Garg, J.; Esfarjani, K.; Jandl, A.; Bulsara, M. T.; Schmidt, A. J.; Minnich, A. J.; Chen, S.; Dresselhaus, M. S.; Ren, Z.; et al. Coherent Phonon Heat Conduction in Superlattices. *Science* **2012**, *338* (6109), 936−939.
(17) Hu, Z. X.; Kong, X. H.; Qiao, J. S.; Normand, B.; Ji, W. Interlayer Electronic Hybridization leads to Exceptional Thickness-dependent Vibrational Properties in Few-layer Black Phosphorus. *Nanoscale* **2016**, *8* (5), 2740−2750.
(18) Dong, S.; Zhang, A. M.; Liu, K.; Ji, J. T.; Ye, Y. G.; Luo, X. G.; Chen, X. H.; Ma, X. L.; Jie, Y. H.; Chen, C. F.; et al. Ultralow-frequency Collective Compression Mode and Strong Interlayer Coupling in Multilayer Black Phosphorus. *Phys. Rev. Lett.* **2016**, *116* (8), 087401.
(19) Ribeiro, H. B.; Pimenta, M. A.; de Matos, C. J. S. Raman Spectroscopy in Black Phosphorus. *J. Raman Spectrosc.* **2018**, *49* (1), 76−90.
(20) Jiang, J. W.; Wang, B. S.; Park, H. S. Interlayer Breathing and Shear Modes in Few-layer Black Phosphorus. *J. Phys.: Condes. Matter* **2016**, *28* (16), 165401.
(21) Ge, S. F.; Liu, X. F.; Qiao, X. A.; Wang, Q. S.; Xu, Z.; Qiu, J.; Tan, P. H.; Zhao, J. M.; Sun, D. Coherent Longitudinal Acoustic Phonon Approaching THz Frequency in Multilayer Molybdenum Disulphide. *Sci. Rep* **2015**, *4*, 5722.
(22) Hudert, F.; Bruchhausen, A.; Issenmann, D.; Schecker, O.; Waitz, R.; Erbe, A.; Scheer, E.; Dekorsy, T.; Mlayah, A.; Huntzinger, J. R. Confined Longitudinal Acoustic Phonon Modes in Free-standing Si Membranes Coherently Excited by Femtosecond Laser Pulses. *Phys. Rev. B* **2009**, *79* (20), 201307.
(23) Creti, A.; Anni, M.; Zavelani-Rossi, M.; Lanzani, G.; Manna, L.; Lomascolo, M. Ultrafast Carrier Dynamics and Confined Acoustic Phonons in CdSe Nanorods. *J. Opt. A-Pure Appl. Opt.* **2008**, *10* (6), 064004.
(24) Miao, X. C.; Zhang, G. W.; Wang, F. J.; Yan, H. G.; Ji, M. B. Layer-dependent Ultrafast Carrier and Coherent Phonon Dynamics in Black Phosphorus. *Nano Lett.* **2018**, *18* (5), 3053−3059.
(25) Baldini, E.; Dominguez, A.; Palmieri, T.; Cannelli, O.; Rubio, A.; Ruello, P.; Chergui, M. Exciton Control in a Room Temperature Bulk Semiconductor with Coherent Strain Pulses. *Sci. Adv.* **2019**, *5* (11), eaax2937.
(26) Babilotte, P.; Morozov, E.; Ruello, P.; Mounier, D.; Edely, M.; Breteau, J. M.; Bulou, A.; Gusev, V. Physical Mechanism of Coherent Acoustic Phonons Generation and Detection in GaAs Semiconductor. *J. Phys.: Conf. Ser.* **2007**, *92*, No. 012019.
(27) Ruello, P.; Gusev, V. E. Physical Mechanisms of Coherent Acoustic Phonons Generation by Ultrafast Laser Action. *Ultrasonics* **2015**, *56*, 21−35.
(28) Thomsen, C.; Strait, J.; Vardeny, Z.; Maris, H. J.; Tauc, J.; Hauser, J. J. Coherent Phonon Generation and Detection by Picosecond Light-pulses. *Phys. Rev. Lett.* **1984**, *53* (10), 989−992.
(29) Park, H.; Wang, X.; Nie, S.; Clinite, R.; Cao, J. Mechanism of Coherent Acoustic Phonon Generation under Nonequilibrium Conditions. *Phys. Rev. B* **2005**, *72* (10), 100301.
(30) Jang, H. J.; Wood, J. D.; Ryder, C. R.; Hersam, M. C.; Cahill, D. G. Anisotropic Thermal Conductivity of Exfoliated Black Phosphorus. *Adv. Mater.* **2015**, *27* (48), 8017−8022.
(31) Ling, X.; Liang, L. B.; Huang, S. X.; Puretzky, A. A.; Geohegan, D. B.; Sumpter, B. G.; Kong, J.; Meunier, V.; Dresselhaus, M. S. Low-frequency Interlayer Breathing Modes in Few-layer Black Phosphorus. *Nano Lett.* **2015**, *15* (6), 4080−4088.
(32) Ge, S. F.; Li, C. K.; Zhang, Z. M.; Zhang, C. L.; Zhang, Y. D.; Qiu, J.; Wang, Q. S.; Liu, J. K.; Jia, S.; Feng, J.; et al. Dynamical Evolution of Anisotropic Response in Black Phosphorus under Ultrafast Photoexcitation. *Nano Lett.* **2015**, *15* (7), 4650−4656.
(33) Ashcroft, N. W.; Mermin, N. D. *Solid State Physics*; Harcourt College: Philadelphia, PA, 1976.
(34) Thomsen, C.; Grahn, H. T.; Maris, H. J.; Tauc, J. Surface Generation and Detection of Phonons by Picosecond Light-pulses. *Phys. Rev. B: Condens. Matter Mater. Phys.* **1986**, *34* (6), 4129−4138.
(35) Meng, S. J.; Shi, H. Y.; Jiang, H.; Sun, X. D.; Gao, B. Anisotropic Charge Carrier and Coherent Acoustic Phonon Dynamics of Black Phosphorus Studied by Transient Absorption Microscopy. *J. Phys. Chem. C* **2019**, *123* (32), 20051−20058.
(36) Bruchhausen, A.; Gebs, R.; Hudert, F.; Issenmann, D.; Klatt, G.; Bartels, A.; Schecker, O.; Waitz, R.; Erbe, A.; Scheer, E.; et al. Subharmonic Resonant Optical Excitation of Confined Acoustic Modes in a Free-standing Semiconductor Membrane at GHz Frequencies with a High-repetition-rate Femtosecond Laser. *Phys. Rev. Lett.* **2011**, *106* (7), 077401.
(37) Groenen, J.; Poinsotte, F.; Zwick, A.; Sotomayor Torres, C. M.; Prunnila, M.; Ahopelto, J. Inelastic Light Scattering by Longitudinal Acoustic Phonons in Thin Silicon Layers: From Membranes to Silicon-on-insulator Structures. *Phys. Rev. B: Condens. Matter Mater. Phys.* **2008**, *77* (4), No. 045420.
(38) Ling, X.; Huang, S. X.; Hasdeo, E. H.; Liang, L. B.; Parkin, W. M.; Tatsumi, Y.; Nugraha, A. R. T.; Puretzky, A. A.; Das, P. M.; Sumpter, B. G.; et al. Anisotropic Electron-photon and Electron-phonon Interactions in Black Phosphorus. *Nano Lett.* **2016**, *16* (4), 2260−2267.
(39) Brillouin, L. Diffusion de La Lumière et Des Rayons X Par Un Corps Transparent Homogène. *Ann. Phys.* **1922**, *9* (17), 88−122.
(40) Morita, A.; Sasaki, T. Electron-phonon Interaction and Anisotropic Mobility in Black Phosphorus. *J. Phys. Soc. Jpn.* **1989**, *58* (5), 1694−1704.
(41) Babilotte, P.; Ruello, P.; Vaudel, G.; Pezeril, T.; Mounier, D.; Breteau, J. M.; Gusev, V. Picosecond Acoustics in P-doped Piezoelectric Semiconductors. *Appl. Phys. Lett.* **2010**, *97* (17), 174103.
(42) Bartels, A.; Dekorsy, T.; Kurz, K.; Kohler, K. Coherent Zone-folded Longitudinal Acoustic Phonons in Semiconductor Superlattices: Excitation and Detection. *Phys. Rev. Lett.* **1999**, *82* (5), 1044−1047.
(43) Babilotte, P.; Ruello, P.; Pezeril, T.; Vaudel, G.; Mounier, D.; Breteau, J. M.; Gusev, V. Transition from Piezoelectric to Deformation Potential Mechanism of Hypersound Photogeneration in N-doped GaAs Semiconductors. *J. Appl. Phys.* **2011**, *109* (6), 064909.
(44) Wang, J. C.; Guo, C. L. Effect of Electron Heating on Femtosecond Laser-induced Coherent Acoustic Phonons in Noble Metals. *Phys. Rev. B* **2007**, *75* (18), 184304.

https://doi.org/10.1021/acs.jpclett.1c01463
J. Phys. Chem. Lett. 2021, 12, 5871−5878